JGR Solid Earth

RESEARCH ARTICLE
10.1029/2019JB017572

Special Section:
Physical Properties of Rocks, Friction and Fracturing: The Walsh Volume

Shale Anisotropy Estimation From Logs in Vertical Wells

Yunyue Elita Li[1], **Arthur C. H. Cheng**[1], **and Nan You**[1]

[1]Department of Civil and Environmental Engineering, National University of Singapore, Singapore

Abstract Anisotropic elastic parameters for shales are widely needed in seismic imaging, reservoir characterization, and carbon sequestration monitoring. Unlike other elastic parameters such as vertical *P* and *S* wave velocities, anisotropy parameters are not measured directly from the acoustic well logs due to the single-directional nature of a well. We assume that shale anisotropy is induced by thin cracks that are filled with liquid in a background isotropic medium, whose bulk and shear moduli are obtained from the vertically measured *P* and *S* wave velocities, density, and porosity from corresponding well logs through a formalized inversion scheme. We show that the estimated anisotropy using the proposed method is consistent with the mineralogy and agrees with the published laboratory measurements. This framework allows us to quantify the uncertainties in the anisotropy parameters estimated from the inversion, which can be used as a measure to evaluate the validity of the chosen rock physics model.

Plain Language Summary The differences in the wave speeds as they propagate in different angles, defined as anisotropy, are widely needed for imaging the subsurface and understanding the tectonic processes. However, measurements made in a vertical borehole cannot provide this directional information. In this study, we assume a rock physics model for shales that adds anisotropy-inducing thin inclusions in an isotropic background, the elastic and fluid properties of which are inverted formally from the measured well logs. The proposed method generates anisotropy estimates that agree with published laboratory measurements and that are consistent with the mineralogy log. Moreover, the proposed method quantifies the uncertainties in the estimated anisotropy, which can be used to evaluate the applicability of the chosen model on a particular rock formation.

Key Points:
- A formalized inversion framework to estimate anisotropy from single-directional well log measurements is proposed
- Parameters inverted from the framework are physically meaningful and bounded
- Uncertainties are quantified based on the framework and indicate the applicability of the chosen rock physics model

Supporting Information:
- Supporting Information S1
- Data Set S1

Correspondence to:
Y. E. Li,
elita.li@nus.edu.sg

Citation:
Li, Y. E., Cheng, A. C. H., & You, N. (2019). Shale anisotropy estimation from logs in vertical wells. *Journal of Geophysical Research: Solid Earth*, *124*, 6602–6611. https://doi.org/10.1029/2019JB017572

Received 20 FEB 2019
Accepted 11 JUL 2019
Accepted article online 24 JUL 2019
Published online 30 JUL 2019

1. Introduction

Shales attract increasing research interests because they play important roles in sedimentary systems as cap rocks of hydrocarbon reservoirs (Vernik & Liu, 1997), seals for carbon sequestration (Vialle et al., 2018), host rocks of nuclear waste disposal (Neuzil, 2013), and unconventional reservoirs of hydrocarbon resources (Jarvie et al., 2007). Shales are intrinsically anisotropic due to the embedding of the clay minerals and inclusions of soft cracks. The importance of elastic anisotropy of shales, in particular vertical transverse isotropy (VTI) with the symmetry axis vertical, has increased dramatically as seismic acquisition demands longer offsets, wider azimuths, and multiple components in exploration and carbon sequestration settings. Besides the strong interests in applied seismology, the tectonic and geodynamic community also investigates seismic anisotropy at a much lower frequency where seismic waves are mostly generated from earthquakes. Seismic anisotropy at such larger scale in deeper section of the crust can provide important insights to the deformation process and the tectonic history (Karato et al., 2008; Zhang et al., 2018).

However, anisotropic model building is a challenging task due to the limited data we can acquire in the field. Although seismic data cover a large area, the accuracy of the velocity and anisotropy models derived from the seismic data inversion is usually too low for direct lithological interpretation. Well log measurements at sparse well locations within a reservoir or at a scientific drilling site, on the other hand, have been used to calibrate the seismic data and to initialize the lithological inversion based on the amplitude-versus-angle measurements. Nonetheless, direct measurements of seismic anisotropy are not available in routine downhole measurements.

Among the commonly available well logging measurements, gamma ray, density, and porosity measurements are measured as nondirectional parameters. Due to the constraints on the trajectory of a well, downhole acoustic measurements are usually single directional, which leads to *P* and *S* wave slowness measured in the vertical direction in most of the wells. Thus, we can easily obtain the two elastic VTI moduli

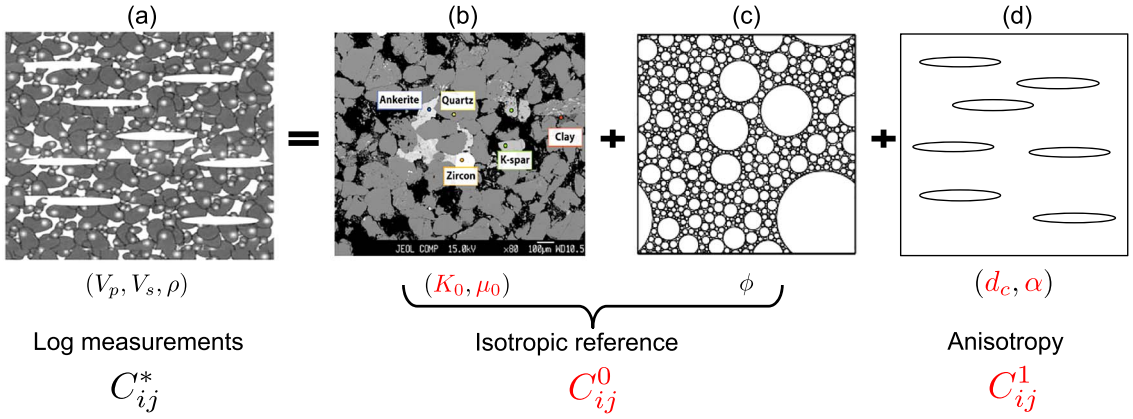

Figure 1. A sketch of the decomposition of (a) a complex rock sample to simple rock physics models: (b) a homogeneous isotropic rock matrix, (c) a set of randomly distributed spherical pores, and (d) a set of aligned thin cracks. Model parameters and moduli are defined in section 2. Variables in black denote commonly available well log measurements, while variables in red denote the unknown model parameters that are not directly measurable.

that are determined by the vertical propagating *P* and *S* waves: $C_{33} = \rho V_p^2$ and $C_{44} = \rho V_{sv}^2$. Recently, Stoneley wave measurements are proposed to be inverted to assess the anisotropic characteristics of a formation, due to their sensitivity to the SH wave, specifically the elastic modulus C_{66}, at the low-frequency limit (Ellefsen et al., 1992; Tang & Cheng, 2004). However, Stoneley waves measurements can be highly variable since a number of other factors such as permeability, borehole rugosity, and borehole mud invasion can affect the measured Stoneley wave velocity. Moreover, Stoneley wave's sensitivity to the SH wave reduces when the formation *S* wave velocity is faster than the borehole fluid *P* wave velocity (Cheng & Toksöz, 1983). In any case, we do not have direct *P* wave anisotropy measurements from the well logs in a vertical well, which is strongly needed by seismic imaging and lithological inversion (Li et al., 2011, 2016).

A common approach to estimate *P* wave anisotropy is to assume a fixed relationship between the different moduli. An example is the ANNIE model (Schoenberg et al., 1996), in which the *P* wave anisotropy is set to be twice the *S* wave anisotropy, or alternatively, the Thomsen parameter δ is set to zero. Modifications to the ANNIE model was proposed by Quirein et al. (2014) based on a specific set of core measurements, but the modifications are empirical rather than model based. Guo et al. (2014) proposed an additional parameter, clay lamination, to build an anisotropic rock physics model, but clay lamination is not a directly measurable parameter.

Many authors (e.g., Bandyopadhyay, 2009; Hornby et al., 1994) have built averaged depth trends based on well log and lab measurements in order to guide seismic processing. Due to the complexity of the rock physics model and the lack of measurements in the data, large uncertainty exists in the rock physics modeling exercises. Therefore, most of the rock physics models describe the qualitative depth trends of anisotropy, without providing quantitative information. Bachrach et al. (2013) and Li et al. (2014) managed to utilize stochastic rock physics modeling schemes to capture the uncertainties in the modeling process and demonstrated that the rock physics modeling results can be used to constrain seismic imaging and inversion. However, due to the arbitrary choices of the parameter distribution and their independency, the resulting rock physics models might be inconsistent across different realizations of the input parameters.

In this paper, we propose to estimate formation anisotropy from vertical and nondirectional measurements assuming a crack rock physics model, which effectively characterizes the formation as a VTI medium. We decompose the rock into three cascaded components as sketched out in Figure 1: (1) a background homogenous isotropic rock matrix, which is fully determined by its mineral components, (2) a randomly distributed spherical pore space saturated with water, and (3) a set of aligned thin cracks that accounts for the VTI anisotropy. To ensure a consistent rock physics model, we set up an inverse problem to estimate the model parameters that are not directly measured by the well logs. A detailed analysis of the inversion show that the formalized inverse problem cannot uniquely determine a single set of parameters needed by the rock physics model. Instead, their uncertainties, and the uncertainties in the resulting anisotropy, are quantified.

We compare the modeled moduli and anisotropy parameters with the published laboratory measurements in Vernik and Liu (1997) and confirm that the proposed modeling method can provide reasonable estimates

for the Thomsen anisotropy parameters ϵ, δ, and γ for a VTI rock model. We apply the workflow using a set of field well log measurements. We compare the modeled anisotropy models with the mineral logs and demonstrate that the modeled anisotropy agrees well with the lithology. Finally, uncertainties of each anisotropy parameter are quantified, which may be used as statistical inputs of subsequent signal processing and a potential measure for the applicability of the chosen rock physics model.

2. Hudson-Cheng's Ellipsoidal Crack Model

Hudson (1981) and Cheng (1993) developed a second-order approximation for the effective moduli of a cracked medium based on ellipsoidal inclusions. Assuming crack density is small in intact shale formations, we neglect the second-order correction to the background moduli in the original formulation and utilize the first-order approximation in this paper. The effective elastic moduli are given by

$$C_{ij}^{*} = C_{ij}^{0} + C_{ij}^{1}, \tag{1}$$

where the effective elastic moduli may be measured with downhole logging tools. C_{ij}^{0} are the moduli of the background, which is assumed isotropic and is consisted of the rock matrix (Figure 1b) and the spherical inclusions of water- or brine-saturated pores (Figure 1c). C_{ij}^{1} are the first-order corrections that are needed due to the penny-shape cracks (Figure 1d). The background moduli are given by

$$\begin{aligned} C_{11}^{0} &= C_{33}^{0} = \lambda + 2\mu, \\ C_{13}^{0} &= \lambda, \\ C_{44}^{0} &= C_{66}^{0} = \mu, \end{aligned} \tag{2}$$

where λ and μ are the Lamé constants of the isotropic reference. The first-order corrections are given by

$$C_{11}^{1} = -\frac{\lambda^2}{\mu} d_c U_3, \tag{3}$$

$$C_{13}^{1} = -\frac{\lambda(\lambda + 2\mu)}{\mu} d_c U_3, \tag{4}$$

$$C_{33}^{1} = -\frac{(\lambda + 2\mu)^2}{\mu} d_c U_3, \tag{5}$$

$$C_{44}^{1} = -\mu d_c U_1, \tag{6}$$

$$C_{66}^{1} = 0, \tag{7}$$

where the crack density $d_c = \frac{3\phi_s}{4\pi\alpha}$ is defined by the ratio of the crack porosity ϕ_s and the aspect ratio α of the ellipsoidal cracks. For fluid-filled weak ($\alpha \ll \frac{K_f}{K_0}$) inclusions,

$$\begin{aligned} U_3 &= \frac{4(\lambda + 2\mu)}{3(\lambda + \mu)} \frac{1}{\beta}, \\ U_1 &= \frac{16(\lambda + 2\mu)}{3(3\lambda + 4\mu)}, \end{aligned} \tag{8}$$

with

$$\beta = \frac{K_f(\lambda + 2\mu)}{\pi\alpha\mu(\lambda + \mu)}, \tag{9}$$

where K_f is the bulk modulus of the fluid and K_0 is the bulk modulus of the background matrix. In a vertical well, P and S wave velocity (V_p and V_s) logs and density (ρ) logs provide measurement for the effective moduli of C_{33}^{*} and C_{44}^{*} (Tang & Cheng, 2004), where

$$\begin{aligned} C_{33}^{*} &= \rho V_p^2, \\ C_{44}^{*} &= \rho V_s^2. \end{aligned} \tag{10}$$

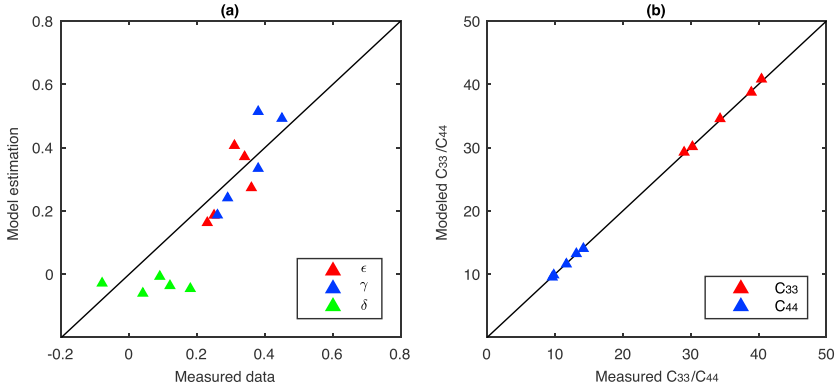

Figure 2. Comparison between model estimations and lab measurements of ϵ, γ, and δ in (a) and C_{33} and C_{44} in (b) with $K_0 = 30.9$ GPa, $\mu_0 = 20.1$ GPa, and $\alpha = 0.032$.

2.1. Background Moduli Estimation by Nonlinear Parameter Inversion

The background moduli can be estimated from the mineral components and the porosity if mineral logs are available. In most cases, however, mineral logs are less available than porosity and density logs in downhole measurements. Assuming an isotropic background, we approximate its moduli by the Hashin-Shtrikman (HS) upper bounds (Hashin & Shtrikman, 1963; Mavko et al., 2009). They are fully defined by the matrix moduli (K_0, μ_0), fluid bulk modulus (K_f), and the porosity (ϕ) as follows:

$$K^{\mathrm{HS+}} = K_0 + \frac{\phi}{(K_f - K_0)^{-1} + (1-\phi)(K_0 + \frac{4}{3}\mu_0)^{-1}}, \tag{11}$$

$$\mu^{\mathrm{HS+}} = \mu_0 + \frac{\phi}{(\mu_f - \mu_0)^{-1} + 2(1-\phi)\frac{K_0+2\mu_0}{5\mu_0(K_0+\frac{4}{3}\mu_0)}}. \tag{12}$$

Further assuming $\lambda = K^{\mathrm{HS+}} - \frac{2}{3}\mu^{\mathrm{HS+}}$ and $\mu = \mu^{\mathrm{HS+}}$, we can solve for the background matrix moduli K_0, μ_0, the crack density d_c, and the aspect ratio α of the ellipsoidal cracks by solving the following nonlinear optimization problem:

$$\min J(K_0, \mu_0, \alpha) = \left\| \frac{\mu C_{33}^1}{(\lambda+2\mu)^2 U_3} - \frac{C_{44}^1}{\mu U_1} \right\|_2^2, \tag{13}$$

which effectively minimizes the differences in the observed and modeled P and S wave vertical velocities. To solve the above inverse problem, a straightforward grid search is applied since the calculations involved are rather trivial. The only tunable parameters for this inversion are the bounds and interval of the search space for each model parameter. The bounds are set wide enough to include all possible values of each model parameter, and the intervals are set small enough to provide sufficient resolution to the final solution. With the solution of the optimization (13), we obtain the full stiffness tensor using equations (3) to (7) and corresponding anisotropy parameters using Thomsen's definition.

Constrained by the P and S wave velocities, inversion for K_0, μ_0, and α may show different sensitivities. Experiments show that the inversion has the best constraint on α and better constraint on K_0 compared with μ_0. The multiparameter distribution obtained by solving equation (13) will help define the correlation of the parameters and reduce the search space when performing stochastic rock physics modeling for anisotropy.

3. Results

In this section we present the results of applying our crack model first to a set of laboratory data from Vernik and Liu (1997) and then to a set of field well log data from China to estimate the anisotropy parameters of a shale formation. The two data sets have no geographical or geological overlap. They are obtained from independent sources. Lastly, we analyze the uncertainties of the inversion results from the field data.

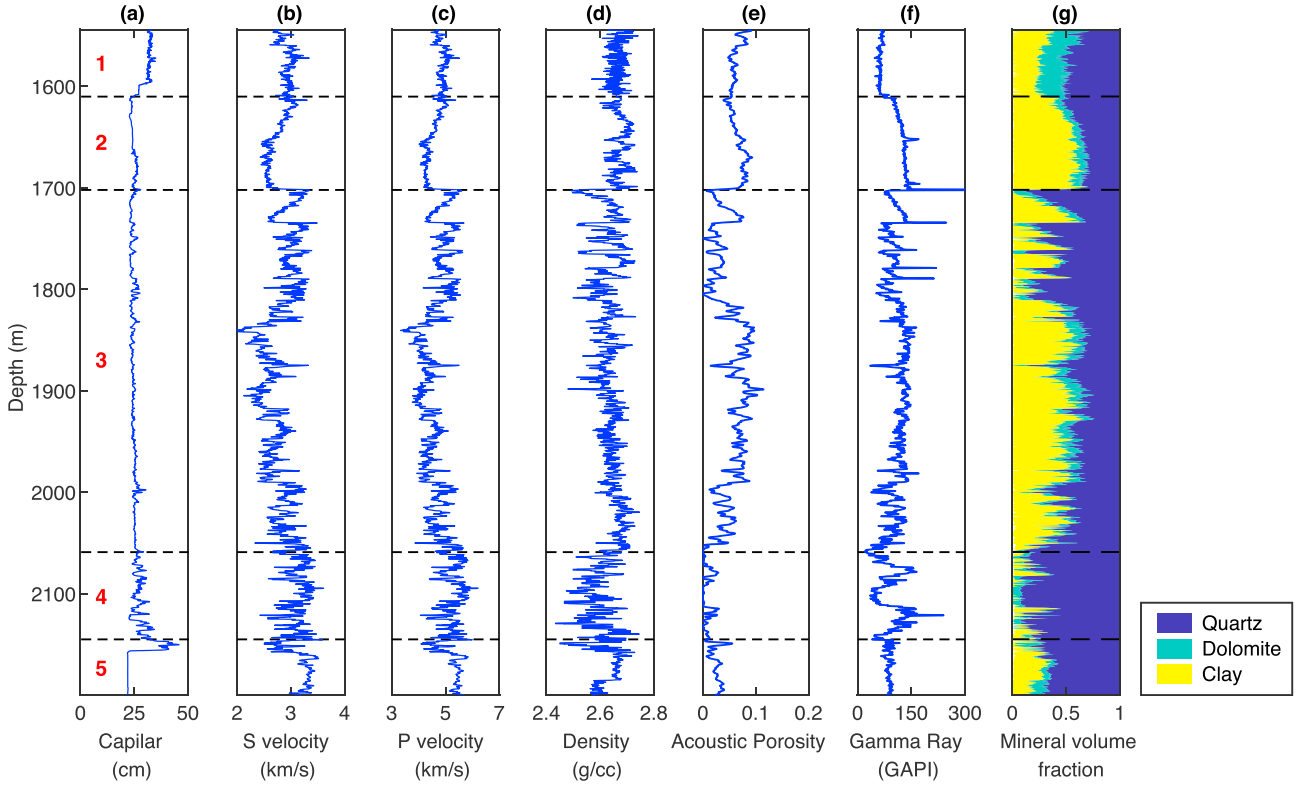

Figure 3. Log measurements of (a) caliper, (b) V_s, (c) V_p, (d) ρ, (e) acoustic porosity, (f) Gamma ray, and (g) volumetric fraction of minerals in a well in Sichuan, China. The back dashed lines denote the lithological layer boundaries.

3.1. Laboratory Data Validation

Vernik and Liu (1997) measured the petrophysical properties (density, porosity, directional velocities, etc.) in the laboratory and derived anisotropy parameters of 20 brine-saturated shale samples from several different geological formations. Since we need to invert for three parameters, at least three independent measurements on a similar shale formation are needed. This requirement leaves us a small subset of five samples from the Bazhenov formation and the inverted K_0, μ_0, and α are 30.9 GPa, 20.1 GPa, and 0.032, respectively.

Figure 2b shows that the modeled and measured C_{33} and C_{44} agree very well with each other, demonstrating the success of achieving our objective defined in equation (13). Figure 2a shows that the modeled ϵ and γ also show reasonable agreement with the measured values, but the modeled δ are consistently smaller than the corresponding measurements. There are two potential reasons for the mismatch in δ. First, lab measurements on δ are often unreliable because of the difficulty of cutting a shale sample at the 45° angle (Bandyopadhyay, 2009). Second, our choice of the Hudson-Cheng model has a larger uncertainty in C_{13} compared with the other elastic moduli. We will further demonstrate the latter point in the log data example.

3.2. Field Well Log Data

We next examine a set of field well log data from Sichuan, China. Subsurface structure revealed by seismic images is fairly flat with sand-shale sequences within a potential shale gas play. From the logs, a shale section can be identified with low porosity, high gamma ray, and rich clay content between depth of 1,544 and 2,200 m. As shown in Figure 3, the shale section can be further subdivided into five layers (separated by the black dashed lines and numbered by 1 to 5 from top to bottom). Each layer displays similarities in log data, including P and S wave velocities, density, porosity, gamma ray, and mineral composition.

Assuming the rock is brine saturated with $K_f = 2.2$ GPa and $\mu_f = 0$, we solve equation (13) to estimate the matrix moduli (K_0, μ_0) and the aspect ratio (α) for each layer using grid search. The range of the search space for each matrix modulus is constrained by the Voigt and Reuss bounds as shown in Table 1. We plot the histograms of K_0, μ_0, and α corresponding to the lowest 2% of the objective function for Layer 3 in

Table 1
Search Range, Inversion Result, and the Uncertainty of the Inverted Parameters for Layer 1–5

	Search range		Inversion result			Average RSD		
Layer	K_0 (GPa)	μ_0 (GPa)	K_0 (GPa)	μ_0 (GPa)	α	C_{11} (%)	C_{66} (%)	C_{13} (%)
1	20.3–59.0	16.4–46.7	43.9	37.2	0.018	10.0	10.2	6.6
2	14.9–44.8	11.4–33.6	37.6	30.3	0.026	5.6	5.7	6.1
3	16.4–48.1	14.1–41.1	40.0	29.4	0.025	5.9	5.6	6.9
4	21.4–50.9	22.3–54.0	48.4	30.6	0.020	3.9	4.6	5.7
5	18.0–50.0	17.3–48.1	44.4	33.2	0.019	4.8	5.6	6.5

Note. RSD = relative standard deviation.

Figures 4a–4c, respectively. Due to the potential noise in the data, we consider all models that fall within the lowest 2% equally probable for the inversion problem. They can also be seen as the marginal probability distribution of the posterior probability of these parameters given the measurements in the well log. Figure 4d shows the objective function map at the optimal α corresponding to the maximum likelihood of its posterior marginal distribution. The topography shows that the objective function is certainly nonconvex, and significant trade-off between K_0 and μ_0 exists in this bivariate distribution.

The red stars in Figures 4a–4d denote the inverted K_0, μ_0, and α, which are chosen to mark the maximum likelihood of the marginal posterior distribution for each parameter. These inverted parameters result in a objective function value that sits well within the lowest 2% range and correspond to a more robust measure of the posterior distribution than the maximum likelihood of the joint distribution. As shown in Figure 4e, given the inverted parameters, the crack densities derived from P and S wave velocities are consistent with each other, and the residual crack density is small. We repeat the same inversion process for the other layers and summarize the resulting K_0, μ_0, and α of Layers 1–5 in Table 1.

Given inversion results in Table 1, we can derive $K^{\mathrm{HS+}}$, $\mu^{\mathrm{HS+}}$, ϵ, γ, δ, and d_c using Hudson-Cheng's model. As shown in Figures 5a and 5b, the estimated $K^{\mathrm{HS+}}$ and $\mu^{\mathrm{HS+}}$ (red lines) are consistently larger than the measured K and μ (black lines). This difference is attributed to the existence of aligned thin cracks, which is quantified as C^1_{ij} in equation (1). The estimated ϵ, γ, and d_c are positively correlated, while the estimated δ oscillates in the near vicinity of 0 (Figures 5c–5e). As expected, the estimated shale anisotropy tends to be stronger at places with higher clay content.

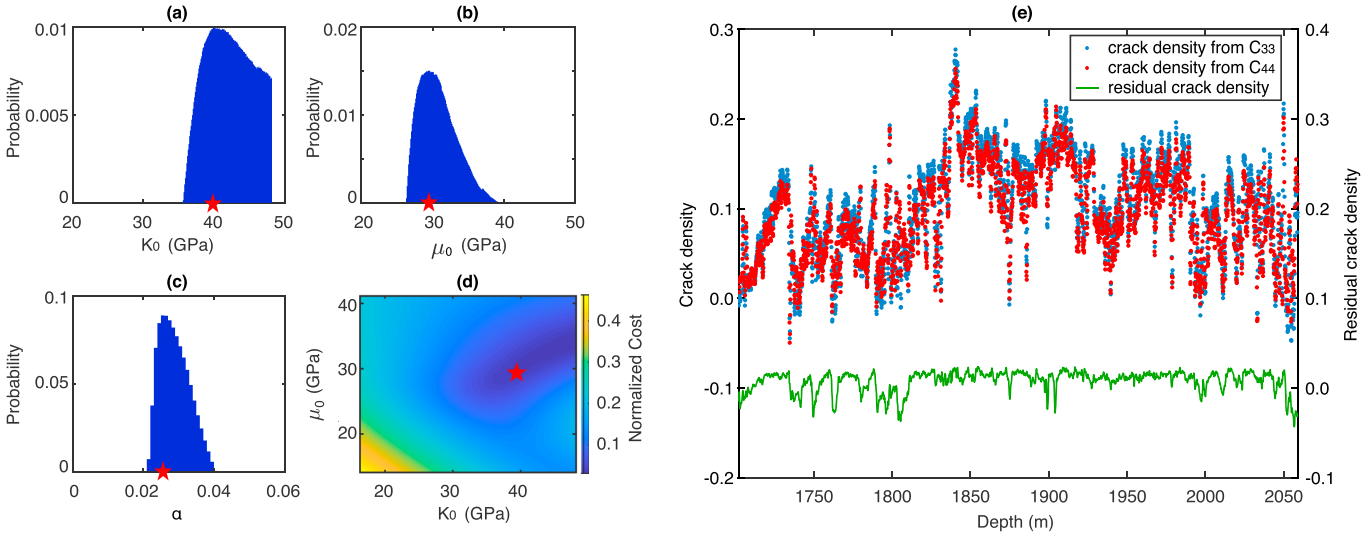

Figure 4. Probability density functions of (a) K_0, (b) μ_0, and (c) α calculated from the models corresponding to the lowest 2% objective function for Layer 3; (d) objective function map at $\alpha = 0.025$; (e) comparison of crack densities from measured C_{33} (blue dots) and C_{44} (red dots) based on inverted parameters of Layer 3 (denoted by the red stars in (a)-(d)), with the green line denoting the difference between these two crack densities.

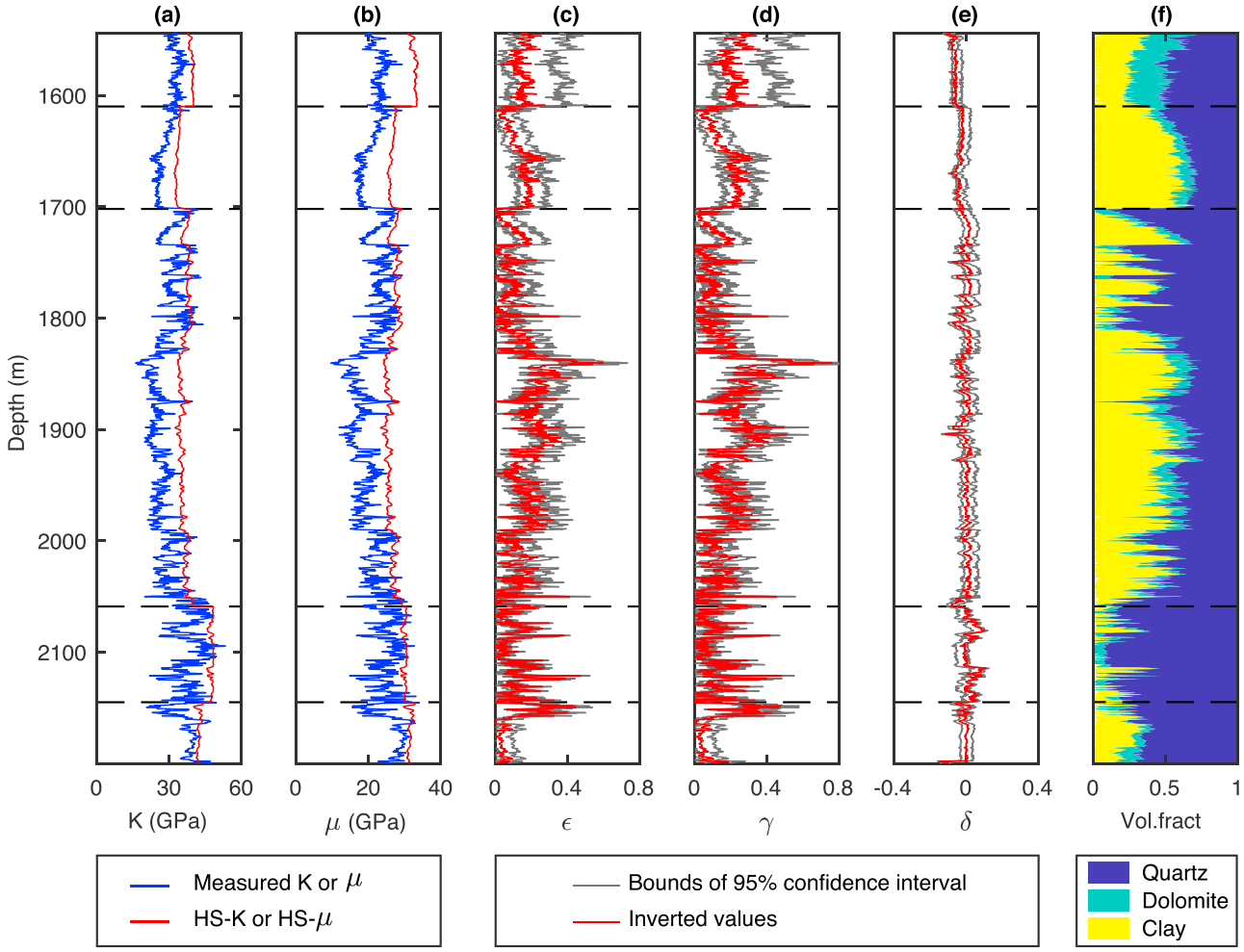

Figure 5. In (a) and (b), comparison between the measured moduli in the vertical direction (blue curves) with the inverted background and isotropic moduli (red curves). The differences between these two curves are attributed to the anisotropy caused by aligned thin cracks. The estimated anisotropy parameters are plotted in (c)–(e) in red and their corresponding 95% confidence intervals are plotted in gray. The estimated anisotropy correlates with the clay content in the mineral log in (f). HS = Hashin-Shtrikman.

3.3. Uncertainty Analysis

As shown in Figure 4d, the inverted K_0 and μ_0 are not uniquely defined given the expected error in the data. Multiple combinations of these parameters can satisfy the objective function equally well. Sampling the joint numerical distribution of K_0 and μ_0 leads to the numerical distributions of the modeled independent moduli (C^*_{11}, C^*_{66}, and C^*_{13}) and finally to the anisotropy parameters, given the measured well logs and the chosen rock physics model.

Figure 6 shows the numerical probability density functions of the modeled moduli (C^*_{11}, C^*_{66}m and C^*_{13}) at one depth within each layer. Distributions of the inverted moduli and the estimated anisotropy can be well approximated by Gaussian distributions, except for the moduli in Layer 1. We approximate a Gaussian distribution for each anisotropy parameter and define the 95% confidence interval for each parameter as ± 2 standard deviations (σ) from the mean ($\bar{x}$). As shown by the gray curves in Figures 5c–5e, our inversion results are within the 95% confidence interval. The uncertainties in the inverted moduli are on the similar level, except for the first layer.

To further quantify the uncertainties, relative standard deviation ($RSD = \frac{\sigma}{\bar{x}}$) is computed for each moduli of C^*_{11}, C^*_{66}, and C^*_{13} at each depth. The mean relative standard deviations for Layers 1–5 are listed in Table 1. Generally, the uncertainties of these moduli are around the same level. Layer 1 is distinguished from the others in that C^*_{11} and C^*_{66} of Layer 1 are about twice more uncertain than those of Layers 2–5. The large uncertainty indicates that the Hudson-Cheng's model may not be appropriate for Layer 1, where an excessive

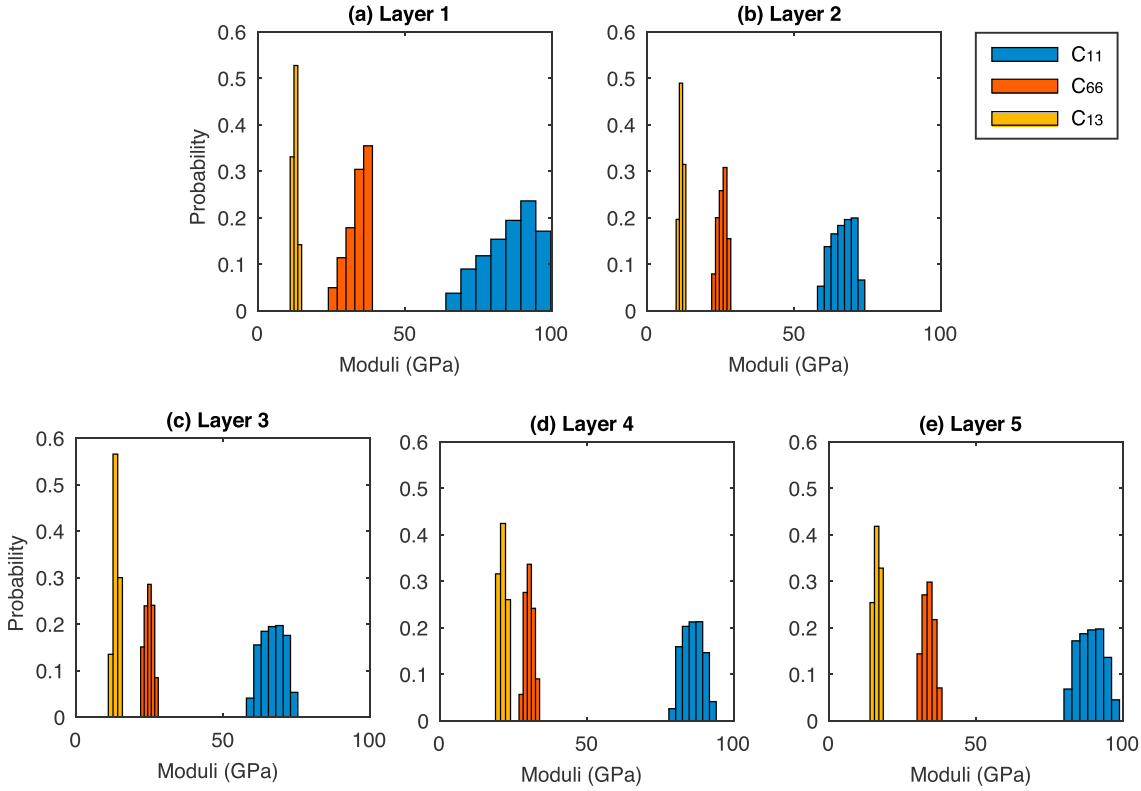

Figure 6. Probability distribution functions of C_{11}, C_{66}, and C_{13} at depth of 1,545, 1,670, 1,900, and 2,100 m within Layers 1–5 (a–e). Distributions of the inverted moduli can be well approximated by a Gaussian distribution, except for the moduli in Layer 1.

amount of dolomite are present in the shaly sand formation. It has been shown that when both clay and dolomite minerals are rich, wireline measurements tend to overestimate porosity (Worden, 1998). In addition, the cementation effect of dolomite could potentially strengthen the rock matrix beyond the HS upper bound. Without accounting for these effects, our simple model here produces estimates that are biased toward stronger anisotropy. The uncertainties in the other inverted parameters (C_{ij} and crack density) are provided in the supporting information Figure S1.

According to Thomsen's definition of the anisotropy parameters, δ is a quadratic function of C^*_{13}, while ϵ and γ are linearly correlated with C^*_{11} and C^*_{66}, respectively. Hence, δ appears more uncertain than ϵ and γ due to the magnification of uncertainty from C^*_{13} to δ. Constraints from other data sets, such as surface seismic data, may help better resolve the anisotropy parameter δ.

4. Discussions and Conclusions

In this paper, we show that directional information about anisotropy can be derived from nondirectional well logs and vertical measurements of the sonic wave velocities, based on the assumption of a crack-inclusion model. The reason that this is possible is that the *S* wave anisotropy is only dependent on the crack density and not on saturation in the crack model. Moreover, elastic anisotropy manifests itself strongest in the vertical direction as deviation from the background isotropic properties. Our method can be applied for dipping formation layers and deviated wells also, with proper constraints for the dip angle in the model. However, when the dip is high or the well deviation is close to horizontal, the acoustic logs are primarily measuring the fast *P* and *S* wave velocities and the sensitivities to anisotropy decrease.

Compared with previously proposed methods (Bachrach et al., 2013; Bandyopadhyay, 2009), our method eliminates the need of estimating parameters that have little practical guidance and does not depend on a fixed assumption of the relationship between *P* and *S* wave anisotropy, as in the ANNIE model (Schoenberg et al., 1996). It represents a formalized workflow with less input parameters, each with clear physical meanings. Estimated anisotropy parameters can be used (after proper filtering and calibration) as initial solutions

to seismic imaging and amplitude-versus-angle inversion algorithms. Multiple realizations and uncertainty analysis of the anisotropy parameters can also be used to construct the covariances among the elastic parameters for seismic inversion (Li et al., 2016).

The anisotropy modeled using the proposed method might be overestimated due to the choice of the Hashin-Shrikman background model, which attributes all the differences between the background and the estimated moduli to the aligned thin cracks. A softer background, composed of both spherical and randomly distributed thin cracks, would reduce the estimated anisotropy in the shale sections. In addition, to estimate the anisotropy due to organic matters in shale, a nonzero modulus should be used for the shear modulus of the pore fluid. When Stoneley wave log is available from the well logs, the inversion will be better constrained because it provides a direct measurement of C^*_{66}. Nonetheless, the framework presented in this paper makes it easy to include all available log measurements, to test different rock physics models, and to quantify the uncertainty in the derived anisotropy.

The inversion framework proposed here can be adapted for applications associated with the Integrated Ocean Drilling Program (e.g., Gilbert & Salisbury, 2011) as well as the Continental Deep Drilling Program (e.g., Rabbel, 1994), the results of which may add important evidence to bridge the laboratory measurements and seismic estimates. However, due to the longer range of the interested depth interval and the increased complexity in geological settings, anisotropic rock physics models that accommodate more complex stress and fluid conditions should be considered in order to achieve realistic estimation of anisotropy in the deeper crust.

Acknowledgments
The authors acknowledge BGP for providing the well log data in the paper. Due to the proprietary nature of the data, a section of the log is provided without depth references in the supporting information. The lab data used in the paper are also provided in the supporting information. The authors acknowledge the EDB Petroleum Engineering Professorship for their financial support. Yunyue Elita Li is also supported by the MOE Tier-1 Grant R-302-000-182-114.

References

Bachrach, R., Osypov, K., Nichols, D., Yang, Y., Liu, Y., & Woodward, M. (2013). Applications of deterministic and stochastic rock physics modelling to anisotropic velocity model building.v *Geophysical Prospecting*, *61*(2), 404–415.

Bandyopadhyay, K. (2009). Seismic anisotropy: Geological causes and its implications to reservoir geophysics. Stanford University.

Cheng, C. (1993). Crack models for a transversely isotropic medium. *Journal of Geophysical Research*, *98*(B1), 675–684.

Cheng, C. H., & Toksöz, M. N. (1983). Determination of shear wave velocities in "slow" formations, *SPWLA 24rd Annual Logging Symposium* (pp. V1–V22). Calgary: Society of Petrophysicists and Well-Log Analysts.

Ellefsen, K. J., Toksöz, M. N., Tubman, K. M., & Cheng, C. H. (1992). Estimating a shear modulus of a transversely isotropic formation. *Geophysics*, *57*(11), 1428–1434.

Gilbert, L., & Salisbury, M. (2011). Oceanic crustal velocities from laboratory and logging measurements of Integrated Ocean Drilling Program Hole 1256D. *Geochemistry, Geophysics, Geosystems*, *12*, Q09001. https://doi.org/10.1029/2011GC003750

Guo, Z., Li, X.-Y., & Liu, C. (2014). Anisotropy parameters estimate and rock physics analysis for the barnett shale. *Journal of Geophysics and Engineering*, *11*(6), 065006.

Hashin, Z., & Shtrikman, S. (1963). A variational approach to the theory of the elastic behaviour of multiphase materials. *Journal of the Mechanics and Physics of Solids*, *11*(2), 127–140.

Hornby, B. E., Schwartz, L. M., & Hudson, J. A. (1994). Anisotropic effective-medium modeling of the elastic properties of shales. *Geophysics*, *59*(10), 1570–1583.

Hudson, J. A. (1981). Wave speeds and attenuation of elastic waves in material containing cracks. *Geophysical Journal of the Royal Astronomical Society*, *64*(1), 133–150.

Jarvie, D. M., Hill, R. J., Ruble, T. E., & Pollastro, R. M. (2007). Unconventional shale-gas systems: The Mississippian Barnett Shale of north-central Texas as one model for thermogenic shale-gas assessment. *AAPG Bulletin*, *91*(4), 475–499.

Karato, S. I., Jung, H., Katayama, I., & Skemer, P. (2008). Geodynamic significance of seismic anisotropy of the upper mantle: New insights from laboratory studies. *Annual Review of Earth and Planetary Sciences*, *36*, 59–95.

Li, Y., Biondi, B., Clapp, R., & Nichols, D. (2016). Integrated VTI model building with seismic data, geologic information, and rock-physics modeling? Part 1: Theory and synthetic test. *Geophysics*, *81*(5), C177—C191.

Li, Y., Mavko, G., & Nichols, D. (2014). Stochastic rock physics modeling for seismic anisotropy, *SEG Technical Program Expanded Abstracts 2014* (pp. 2899–2904). Colorado, USA: Society of Exploration Geophysicists.

Li, Y., Nichols, D., Osypov, K., & Bachrach, R. (2011). Anisotropic tomography using rock physics constraints. In *73rd EAGE Conference and Exhibition incorporating SPE EUROPEC 2011* (pp. 389–393). Vienna, Austria.

Mavko, G., Mukerji, T., & Dvorkin, J. (2009). *The rock physics handbook: Tools for seismic analysis of porous media*. Cambridge: Cambridge University Press.

Neuzil, C. (2013). Can shale safely host us nuclear waste? *Eos, Transactions American Geophysical Union*, *94*(30), 261–262.

Quirein, J., Eid, M., & Cheng, A. (2014). Predicting the stiffness tensor of a transversely isotropic medium when the vertical Poisson's ratio is less than the horizontal Poisson's ratio, *SPWLA 55th Annual Logging Symposium* (pp. 11). Abu Dhabi: Society of Petrophysicists and Well-Log Analysts.

Rabbel, W. (1994). Seismic anisotropy at the continental deep drilling site (Germany). *Tectonophysics*, *232*(1-4), 329–341.

Schoenberg, M., Muir, F., & Sayers, C. (1996). Introducing ANNIE: A simple three parameter anisotropic velocity model for shales. *Journal of Seismic Exploration*, *5*, 35–49.

Tang, X.-M., & Cheng, C. H. A. (2004). *Quantitative borehole acoustic methods* (Vol. 24). Amsterdam: Elsevier.

Vernik, L., & Liu, X. (1997). Velocity anisotropy in shales: A petrophysical study. *Geophysics*, *62*(2), 521–532.

Vialle, S., Ajo-Franklin, J., & Carey, J. W. (2018). *Geological carbon storage: Subsurface seals and caprock integrity* (Vol. 238). John Wiley & Sons.

Worden, R. H. (1998). Dolomite cement distribution in a sandstone from core and wireline data: The Triassic fluvial Chaunoy Formation, Paris Basin. *Geological Society, London, Special Publications*, *136*(1), 197–211.

Zhang, H., Li, Y. E., Zhao, D., Zhao, J., & Liu, H. (2018). Formation of rifts in Central Tibet: Insight from P wave radial anisotropy. *Journal of Geophysical Research: Solid Earth*, *123*, 8827–8841. https://doi.org/10.1029/2018JB015801